View metadata, citation and similar papers at core.ac.uk

brought to you by CORE

provided by Repositório Científico do Instituto Politécnico do Porto

Available online at www.sciencedirect.com

ScienceDirect

Procedia Manufacturing 38 (2019) 940–947

Procedia MANUFACTURING

www.elsevier.com/locate/procedia

29th International Conference on Flexible Automation and Intelligent Manufacturing (FAIM2019), June 24-28, 2019, Limerick, Ireland.

Comparison of different test configurations for the shear fracture toughness evaluation of a ductile adhesive

A.J.S. Leal[a], R.D.S.G. Campilho[a,b,*], F.J.G. Silva[a], D.F.O. Silva[a], F.J.P. Moreira[a]

[a]*ISEP-School of Engineering, Rua Dr. António Bernardino de Almeida 431, 4200-072 Porto, Portugal*
[b]*INEGI, Campus da FEUP, Rua Dr. Roberto Frias 400, 4200-465 Porto, Portugal*

Abstract

Cohesive zone modelling (CZM) is widely used for predicting the strength of adhesive joints. The key variable for crack path modelling is the critical strain energy release rate (G_C), which can be separated into the tensile (G_{IC}) and shear (G_{IIC}) components. In shear, the End Notched Flexure (ENF) test is widespread. However, other test methods exist and could be a viable replacement. This work aims to make a numerical evaluation between the ENF and Four-Point End Notched Flexure (4ENF) tests to determine G_{IIC} of a ductile adhesive (SikaForce® 7752) and to provide shear CZM laws for further application in design. An inverse technique was used to obtain the shear CZM laws of the adhesive. It was concluded that the G_{IIC} values obtained by the ENF and 4ENF tests are in good agreement. The numerical analysis led to unique shear CZM laws for both tests, with similar results.

© 2019 The Authors. Published by Elsevier B.V.
This is an open access article under the CC BY-NC-ND license (http://creativecommons.org/licenses/by-nc-nd/4.0/)
Peer-review under responsibility of the scientific committee of the Flexible Automation and Intelligent Manufacturing 2019 (FAIM 2019)

Keywords: Adhesive joint; cohesive zone modelling; fracture toughness; cohesive strength; Finite Element Method.

1. Introduction

The accurate strength prediction of bonded joints is vital for the reliable application of this joining method. Damage mechanics and fracture mechanics techniques, weighted against continuum mechanics techniques, usually work well

* Corresponding author. Tel.: +351-939526892; fax: +351-228321159.
E-mail address: raulcampilho@gmail.com

2351-9789 © 2019 The Authors. Published by Elsevier B.V.
This is an open access article under the CC BY-NC-ND license (http://creativecommons.org/licenses/by-nc-nd/4.0/)
Peer-review under responsibility of the scientific committee of the Flexible Automation and Intelligent Manufacturing 2019 (FAIM 2019)
10.1016/j.promfg.2020.01.177

in structures with singularities or in materials that exhibit plastic behaviour. CZM is a widely used method for predicting the strength of adhesive joints, based on both continuum mechanics and fracture principles [1]. It has the advantage that it does not need to have an initial defect for damage evolution to take place. In this technique, the triangular damage law is the most used, although a trapezoidal damage law is more suitable for ductile adhesives [2]. By fracture mechanics techniques in general, the key variable for crack path modelling is G_C, which can be further separated into the G_{IC} and G_{IIC} components. In real life applications, bonded joints are often loaded by a mix of normal and shearing forces, which is called a mixed-mode loading. Under tensile loading, the Double-Cantilever Beam (DCB) and Tapered Double-Cantilever Beam (TDCB) fracture test configurations are the most applied [3]. Under shear loads, the ENF test is generally chosen by researchers [4], because of the simplicity of its application. However, it can be affected by unstable propagation of cracks, leading to a low accuracy in measuring G_{IIC}. Test methods are though available that promote a stable propagation of cracks, such as 4ENF [5]. The Asymmetric Double-Cantilever Beam (ADCB), Mixed-Mode Flexure (MMF) and Mixed-Mode Bending (MMB) are the most used tests for mixed-mode conditions [6]. An accurate estimation of the fracture-driving parameters is fundamental to predict their behaviour. On the other hand, defects or imperfections are often present in bonded joints. The methods based on fracture principles allow modelling these types of flaws and check whether or not they will propagate unstably and cause the structure's collapse [7]. When considering the ENF test to estimate G_{IIC}, some data reduction methods need measuring the crack length (a), while other methods are based on an equivalent crack length or the J-integral. The Compliance Calibration Method (CCM), Direct Beam Theory (DBT) and Corrected Beam Theory (CBT) are some of the most widespread methods needing to measure a. The Compliance-Based Beam Method (CBBM) is a well-known method based on an equivalent crack length (a_{eq}). For the 4ENF test, the CCM (depending on a), and the CBT and the Effective Crack Method (ECM), where the value of a during the test is not necessary, are commonly used.

The standardized ENF, 4ENF and End Loaded Split (ELS) test methods for composite materials were already tested with good results for bonded joints [8]. However, there is not a great abundance of information on the comparison between the ENF and 4ENF tests for G_{IIC} estimation of bonded joints, unlike happens for composite materials. de Morais and Pereira [9] developed a comparison between the ENF and 4ENF tests, in order to validate the ECM to predict the interlaminar G_{IIC} of unidirectional carbon-epoxy laminates. The experimental data showed that crack onset in the 4ENF test is more stable when compared to the ENF test. Comparing the load-displacement (P-δ) curves revealed crack growth at a constant P for the 4ENF test and also higher peak P during the test (approximately 17%) compared to the ENF test. The ECM applied to the ENF specimens allowed to obtain very positive results, despite the unstable beginning of crack. The specimen geometry effect was almost inexistent in the ENF specimen, and it was practically eliminated after crack onset. It was though noted that G_{IIC} for the ENF under predicted those of the 4ENF tests. On the other hand, the friction effects associated to the 4ENF test led to higher specimen stiffness.

This work aims to make a numerical evaluation between the ENF and 4ENF tests to determine G_{IIC} of a ductile adhesive (SikaForce® 7752) and to provide shear CZM laws for further application in design. An inverse technique was used to obtain the shear CZM laws of the adhesive.

2. Experimental details

2.1. Materials

For the adherends, a high tensile yield stress (σ_y) aluminium alloy AA6082 T651 was selected. This aluminium alloy is characterized by high ductility and strength, to avoid the adherends' plasticization. As can be seen in the previous work of Campilho et al. [10], the selected alloy has the following mechanical characteristics: Young's modulus (E) of 70.07±0.83 GPa, σ_y of 261.67±7.65 MPa, tensile failure strength (σ_f) of 324.00±0.16 MPa and tensile failure strain (ε_f) of 21.70±4.24%. A ductile polyurethane adhesive (Sikaforce® 7752) was selected to make the comparative evaluation between the ENF and 4ENF test geometries. Recently, a study was done [11] to characterise this adhesive in terms of mechanical and fracture behaviour. Using bulk tensile tests, the tensile mechanical properties of the adhesives (E, σ_y, σ_f and ε_f) were estimated. On the other hand, the shear mechanical properties were estimated from Thick-Adherend Shear Tests (TAST). To obtain, respectively, G_{IC} and G_{IIC} using conventional data reduction schemes, DCB and ENF tests were used. Table 1summarizes the relevant mechanical and fracture data of the adhesive.

Table 1. Mechanical and fracture properties of the Sikaforce® 7752 [11].

Property	7752
Young's modulus, E [GPa]	0.49±0.09
Poisson's ratio, ν	0.30 [a]
Tensile yield stress, σ_y [MPa]	3.24±0.48
Tensile strength, σ_f [MPa]	11.48±0.25
Tensile failure strain, ε_f [%]	19.18±1.40
Shear modulus, G [GPa]	0.19±0.01
Shear yield stress, τ_y [MPa]	5.16±1.14
Shear strength, τ_f [MPa]	10.17±0.64
Shear failure strain, γ_f [%]	54.82±6.38
Toughness in tension, G_{IC} [N/mm]	2.36±0.17
Toughness in shear, G_{IIC} [N/mm]	5.41±0.47

[a] manufacturer's data

2.2. Joint geometries, manufacturing and testing

The dimensions of the ENF tests are presented in Fig. 1 (a). The relevant parameters are the mid-span L=100 mm, initial crack length a_0≈60 mm, adherends' thickness h=3 mm, width B=25 mm and adhesive thickness t_A=0.2 mm. Fig. 1 (b) relates to the 4ENF tests, and the dimensions are as follows: L=130 mm, loading span L_i=130 mm, a_0≈60 mm, h=3 mm, B=15 mm and t_A=0.2 mm.

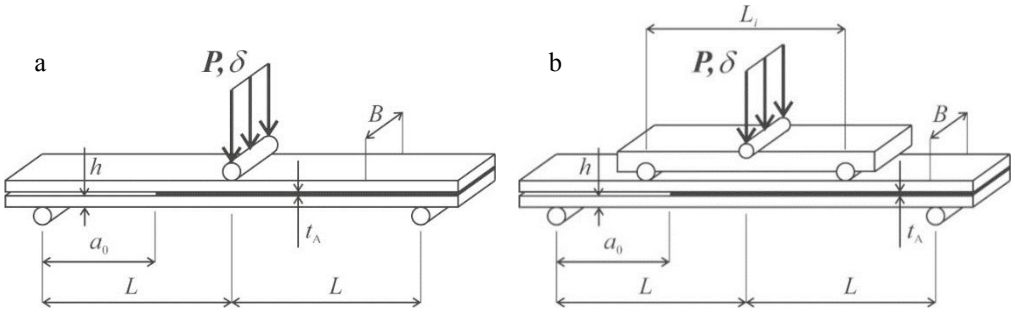

Fig. 1. (a) geometry and dimensions of the ENF and (b) 4ENF joints.

For both tests, the joints were manufacturing in a laboratory under controlled temperature and humidity. Initially, the specimens' faces to bond were roughened by grit blasting and afterwards combined with acetone. A steel jig was used to align the adherends' and calibrated spacers used to enforce t_A. These spacers are composed of a razor blade (thickness of 0.1 mm) between 0.05 mm calibrated sheet strips, thus attaining a total thickness of 0.2 mm (Fig. 2).

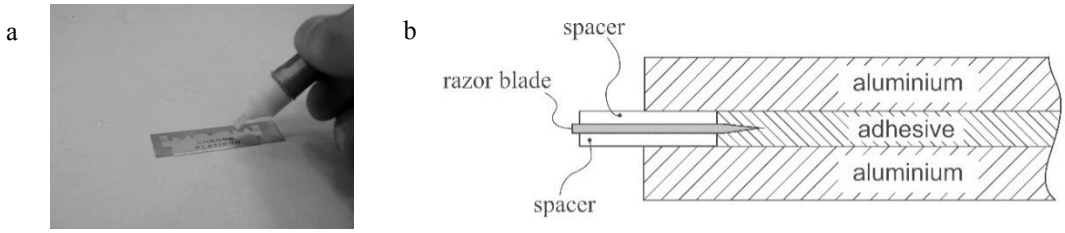

Fig. 2. (a) gluing of crack tip spacer and (a) schematics of the crack tip spacer.

These parts are glued together and then coated with demoulding agent. Final preparation took place by trimming the excess adhesive, cleaning the side faces and painting with brittle corrector fluid. A scale was finally attached to one of the adherends side faces to measure a [12]. Seven samples were prepared for each test type (ENF and 4ENF).

These tests were performed in a controlled environment in a Shimadzu AG-X 100 electro-mechanical testing machine equipped with a 100 kN load cell. An 18 MPixel digital camera was used during the tests to measure a.

3. G_{IIC} data reduction methods

3.1. ENF specimen

Different G_{IIC} data reduction methods are available for the ENF specimens, although in this work only the CBBM was used. The CBBM takes advantage of a_{eq}, calculated using the P-δ curve. It includes in the formulation the damage zone that naturally develops around the crack tip arising from plasticization effects. By this method, G_{IIC} is defined as

$$G_{IIC} = \frac{9P^2 a_{eq}{}^2}{16B^2 E_f h^3} \tag{1}$$

in which E_f is the equivalent flexural modulus of a given specimen, defined using the initial compliance ($C=\delta/P$) of the P-δ curve and value of a_0.

3.2. 4ENF specimen

There are mainly two methods to estimate G_{IIC} for the 4ENF test: (1) the CCM, which requires measuring a, and (2) the CBT, for which this step is not necessary. The CCM consists of applying the Irwin-Kies expression [13]

$$G_{IIC} = \frac{P^2}{2B}\frac{dC}{da} \tag{2}$$

However, for the 4ENF test, C=f(a) becomes a straight line. Thus, the formula is reduced to [14]

$$G_{IIC} = \frac{P^2}{2B} \times C_1 \tag{3}$$

The CBT expression with friction coefficient (μ) correction is given as [5]

$$G_{IIC} = \frac{9P^2\left(2L - L_i\right)^2}{64E_x B^2 h^3}\left(1 - \frac{8\mu h}{3s} + \frac{16\mu^2 h^2}{9s^2}\right) \tag{4}$$

where E_x represents the adherends' Young's modulus along the specimens' length and s=(2L-L_i)/2.

4. Numerical work

4.1. Numerical settings and inverse procedure

Finite Element (FE) simulations of the ENF and 4ENF tests were done in Abaqus®, using an implicit solver (i.e. Abaqus® standard analysis). The analyses were two-dimensional (2D) and geometrically non-linear. A mesh example is given in Fig. 3 for the ENF specimen. Four-node cohesive elements (COH2D4 from Abaqus®) with a triangular shape were considered for the adhesive layer. The adherends were modelled with four-node plane-strain solid FE elements (CPE4 from Abaqus®). Mesh size grading effects, i.e. bias effects, were employed to improve the models' calculation efficiency. As boundary conditions, the supporting cylinders were fixed in the xy plane and the rigid beam was restrained in the horizontal direction and allowed to move down to apply the load. To conclude the models, all contacting surfaces were paired with surface interactions: between the cylinders and the specimen, and between the un-bonded faces of the specimens, i.e. at the pre-crack region, to avoid their interpenetration.

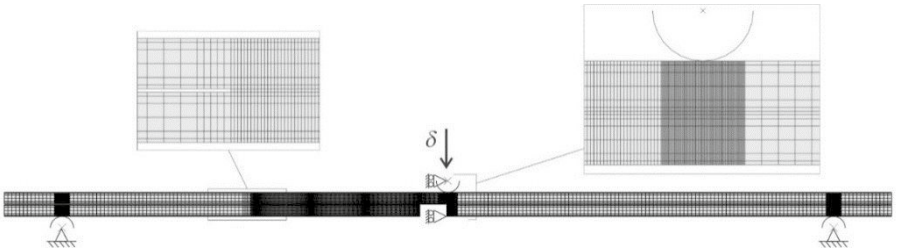

Fig. 3. Mesh refinement for an ENF specimen.

In the numerical analysis, individual models were created for each specimen (either ENF or 4ENF), by including the specific dimensions and a_0 of each specimen. Also, for each specimen, a shear cohesive law was built that included the CBBM G_{IIC} value measured for that particular specimen. As an approximation, the shear cohesive strength (t_s^0) was initially considered as the shear strength (τ_f); see Table 1. The final shear cohesive law of each specimen was found by iteratively fitting the experimental and numerical P-δ curves of the specimens up to the best possible match.

4.2. Triangular CZM formulation

Relationships among stresses and relative displacements linking similar nodes of cohesive elements are the fundament of the CZM. Additionally, those relations (often entitled CZM laws) may be established in pure and mixed mode and make possible to capture the material's behaviour up to failure [15]. This study relies on triangular pure and mixed-mode laws to model the adhesive layer. Under pure-mode loading, damage initiation occurs when the cohesive strength in tension (t_n^0) or t_s^0 is attained, i.e., the material's elastic behaviour is cancelled and degradation starts [16]. Furthermore, the crack propagates up to the adjacent pair of nodes when the values of current tensile or shear cohesive stresses (t_n or t_s, respectively) become null. Under mixed-mode loading, stress and/or energetic criteria are often used to combine the pure-mode laws, and damage begins when the mixed mode cohesive strength (t_m^0) is reached [17]. Several criteria are available for damage initiation and growth when the analysis encompasses mixed-mode loadings. Nevertheless, this study focused on the quadratic nominal stress criterion and a linear power law form for the damage initiation and growth, respectively. This model is described in detail in the work of Rocha and Campilho [18]. The adhesive's properties used in Abaqus® were obtained from Table 1.

5. Results

This Section summarizes all G_{IIC} results from the experimental tests. The CZM study then addresses the estimation of the shear CZM laws of all tests (both ENF and 4ENF) by the inverse technique which, if positively validated can be further used in strength prediction of bonded joints.

5.1. Experimental G_{IIC} results

Experimental testing was undertaken following the description given in Section 2.2. In the case of the ENF test, the tests were run until the crack reached the middle loading cylinder. For the 4ENF joints, the tests were stopped when the crack reached the end of the constant bending moment region. A verification after performing the tests was done to conclude that all specimens failed cohesively in the adhesive during the full extent of crack propagation. Crack growth was smooth and without load jumps, which is characteristic of ductile adhesives such as the Sikaforce® 7752, and it caused a P reduction in the respective P-δ curves. For the ENF specimens, only the CBBM method was evaluated, despite other methods are available in the literature, because of difficulties in the measurement of a during the test. Actually, the white paint cracked before the real crack propagation, which would lead to G_{IIC} measurement errors for methods relying on a. Fig. 4 (a) gives an example of R-curve for the ENF test. G_{IIC} was assumed to be the average G_{II} over the steady crack growth portion of the respective R-curve [19]. Table 2 summarizes the G_{IIC} values (in N/mm) for the Sikaforce® 7752 tested by the ENF and 4 ENF specimens (the latter to be addressed further).

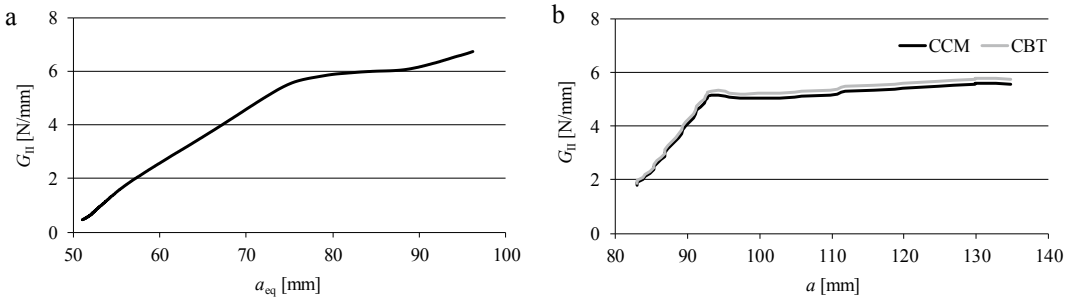

Fig. 4. (a) example *R*-curves for an ENF and (b) 4ENF specimen.

Table 2. G_{IIC} [N/mm] for the Sikaforce® 7752 by the 4ENF test.

	ENF	4ENF		
Specimen		CCM	CBT (μ=0)	CBT (μ=9)
1	5.825	-	-	-
2	5.877	5.276	9.629	5.472
3	5.474	5.425	9.122	5.184
4	4.813	-	-	-
5	5.676	5.293	9.632	5.474
6	5.648	5.555	9.366	5.322
7	5.619	5.318	7.983	4.536
Average	5.562	5.373	9.146	5.198
Deviation	0.356	0.117	0.684	0.389

The P-δ curves' for the 4ENF tests develop significantly different to those of the ENF tests, in the sense that crack propagation happens with a constant load [20]. This difference to the ENF tests occurs because here crack grows in the middle of the loading cylinders, were the bending moment is constant. In this test, the CCM technique relies on measuring dC/da during the crack propagation, which requires plotting the C=f(a) curve, and then differentiating. Fig. 4 (b) presents example *R*-curves for the 4ENF test, considering both CCM and CBT methods, this last after friction coefficient (μ) correction. This μ correction was applied to the *R*-curves by the CBT, which does not require measurement of *a,* to account for the significant effects of friction between cracked faces of adhesive [14].

Table 2 also presents the G_{IIC} values in N/mm for the 4ENF tests. The use of some specimens was not possible because of experimental problems that resulted in much different results compared to the average. The percentile standard deviation was smaller than 10%. Comparing the CCM and the CBT (with μ=0) it is possible to observe that the uncorrected CBT greatly exceeds the CCM values and, in average, G_{IIC} for the CBT (μ=0) was higher than the CCM by 70.2%. Through a visual inspection of the 4ENF tests during crack growth, it was observed that large friction between the cracked faces of the adhesive layer takes place. This effect results from the compression applied to the cracked faces, which have high roughness, leading to an artificial increase of G_{IIC}. The μ value presented in Table 2 was obtained by an iterative procedure conducted by the adjustment of the CBT *R*-curves until they matched those of the CCM. The obtained μ value shows that the CBT is not adjusted for this test configuration.

5.2. Numerical assessment of the shear fracture tests

The methodology specified in Section 4.1 was applied to all ENF and 4ENF specimens. Fig. 5 (a) gives an example of the final experimental and numerical P-δ curves for the ENF test, after the fitting process. It is clear that the final shear cohesive law managed to accurately reproduce the experimental curve. Despite this fact, less smooth experimental crack propagation was found in some specimens, while in the numerical simulations this takes place more stably. In all experimental ENF specimens bonded with the Sikaforce® 7752, the agreement was good and in line with the results of Fig. 5 (a), although triangular CZM laws may not be the best choice to model ductile adhesives. However, when considering fracture tests in particular, since the P-δ and *R*-curves are driven by the fracture energies,

and since crack growth occurs under identical stress conditions, these are independent of the CZM law shape. After the fitting process, t_s^0=19.0±1.7 MPa was found by averaging all ENF specimens. The shear CZM laws resulting from the ENF tests' fitting process are presented in Fig. 5 (b). It is clear that some changes to t_s^0 were required to achieve good results. Despite this fact, the average curve is not too offset to the individual curves. If the aforementioned average t_s^0 is compared to τ_f (Table 1), the difference is +86.8%. This difference is discussed in previous works [21] and it arises from adhesive behaviour' dependence on the restraining effects caused by the adherends.

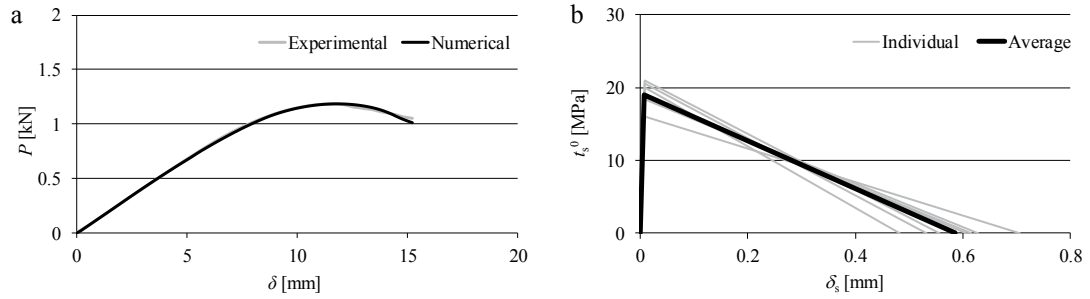

Fig. 5. (a) example of the P-δ curves' fitting procedure for one ENF specimen and (b) shear CZM laws obtained by inverse fitting for the ENF test: individual and average curves.

A parallel study was performed for the 4ENF specimens, and an example of P-δ curves' fitting is given in Fig. 6 (a). Also in this case it was possible to provide a good match, either in the pre-cracking or cracking stages. Nonetheless, some oscillation was detected in the experimental curves, due to experimental effects. Here, t_s^0=19.0±2.3 MPa were the obtained values resulting from the fitting process. The offset between t_s^0 and τ_f, this last one presented in Table 1 is, identically to the ENF results, of +86.8%.

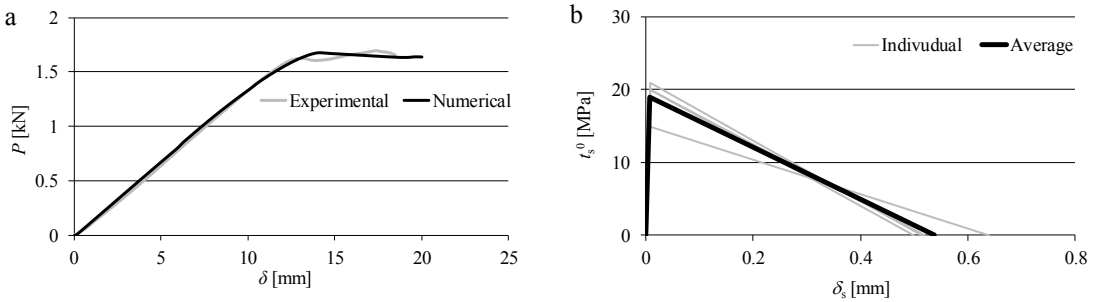

Fig. 6. (a) example of the P-δ curves' fitting procedure for one 4ENF specimen and (b) shear CZM laws obtained by inverse fitting for the 4ENF test: individual and average curves.

Fig. 6 (b) gives the individual shear CZM laws deriving from the inverse procedure and average law. A comparison between ENF (Fig. 5 b) and 4ENF (Fig. 6 b) shear CZM laws shows that the 4ENF scatter is smaller. The offset between the individual and average curve is also reduced for the 4ENF specimens. The t_s^0 values are extremely close, except for a single specimen. In the end, both ENF and 4ENF specimens provided close shear CZM laws.

6. Conclusions

The work presented here numerically evaluated the ENF and 4ENF tests to estimate G_{IIC} of a ductile structural adhesive. Within this scope, the shear CZM laws were validated against experiments and compared between the two test methods, such that they could be used in the design of bonded joints. ENF data analysis was accomplished by the

CBBM, while the 4ENF data was addressed by the CCM and CBT. Moreover, one reduction method for each test would produce results without the requirement to measure a, which is a clear advantage. The CBBM G_{IIC} results for the ENF revealed similar values between specimens. For the 4ENF test, the CBT without μ correction gave offset results and, to provide comparable results with the CCM, extremely high μ were required. The CZM technique was then applied to the estimation of the shear CZM laws of each specimen, by using an inverse technique. For both ENF and 4ENF tests, the scatter between CZM laws was small, which attested the robustness of the employed method. The experimental P-δ curves of the ENF specimens were precisely replicated, whilst in the 4ENF specimens the agreement was good, but with minor deviations to the experimental curve. This occurred due to problems in the P-δ curves' adjustment arising from the higher sensitivity to the CZM law shape. A direct comparison between the two test methods shows that the ENF test accurately estimates G_{IIC} by the CBBM, the machine setup is simpler and it involves low friction. However, unstable crack growth can occur, even though it was not found in this work. The 4ENF test, on the other hand, it ensures stable crack growth, but only few works in the literature use this method. As disadvantages, only the CCM, requiring a measurement, can produce comparable results, and the machine setup is more elaborated due to using two loading cylinders. As a final recommendation, the ENF test presents a higher potential than the 4ENF test, although good results were also found with the 4ENF-CCM.

References

[1] J. Jang, M. Sung, S. Han, W.-R. Yu, Prediction of delamination of steel-polymer composites using cohesive zone model and peeling tests, Composite Structures, 160 (2017) 118-27.
[2] C.D.M. Liljedahl, A.D. Crocombe, M.A. Wahab, I.A. Ashcroft, Damage modelling of adhesively bonded joints, International Journal of Fracture, 141 (2006) 147-61.
[3] B.R.K. Blackman, A.J. Kinloch, M. Paraschi, W.S. Teo, Measuring the mode I adhesive fracture energy, GIC, of structural adhesive joints: the results of an international round-robin, International Journal of Adhesion and Adhesives, 23 (2003) 293-305.
[4] J.C.S. Azevedo, R.D.S.G. Campilho, F.J.G. da Silva, T.M.S. Faneco, R.M. Lopes, Cohesive law estimation of adhesive joints in mode II condition, Theoretical and Applied Fracture Mechanics, 80 (2015) 143–54.
[5] W.-X. Wang, M. Nakata, Y. Takao, T. Matsubara, Experimental investigation on test methods for mode II interlaminar fracture testing of carbon fiber reinforced composites, Composites Part A: Applied Science and Manufacturing, 40 (2009) 1447-55.
[6] F.J.P. Chaves, L.F.M. da Silva, M.F.S.F. de Moura, D.A. Dillard, V.H.C. Esteves, Fracture Mechanics Tests in Adhesively Bonded Joints: A Literature Review, The Journal of Adhesion, 90 (2014) 955-92.
[7] L.F.M. da Silva, R.D.S.G. Campilho. Advances in numerical modelling of adhesive joints. Heidelberg: Springer; 2012.
[8] L.F.M. da Silva, D.A. Dillard, B. Blackman, R.D. Adams. Testing Adhesive Joints. Wiley-VCH Verlag & Co.; 2012.
[9] A.B. de Morais, A.B. Pereira, Application of the effective crack method to mode I and mode II interlaminar fracture of carbon/epoxy unidirectional laminates, Composites: Part A: applied science and manufacturing, 38 (2006) 785–94.
[10] R.D.S.G. Campilho, M.D. Banea, A.M.G. Pinto, L.F.M. da Silva, A.M.P. de Jesus, Strength prediction of single- and double-lap joints by standard and extended finite element modelling, International Journal of Adhesion and Adhesives, 31 (2011) 363-72.
[11] T. Faneco, R. Campilho, F. Silva, R. Lopes, Strength and Fracture Characterization of a Novel Polyurethane Adhesive for the Automotive Industry, Journal of Testing and Evaluation, 45 (2017) 398-407.
[12] M.D. Banea, L.F.M. Da Silva, R.D.S.G. Campilho, The Effect of Adhesive Thickness on the Mechanical Behavior of a Structural Polyurethane Adhesive, The Journal of Adhesion 91 (2014) 331-46.
[13] P. Compston, P. Jar, P. Burchill, K. Takahashi, The effect of matrix toughness and loading rate on the mode-II interlaminar fracture toughness of glass-fibre/vinyl-ester composites, Composites Science and Technology, 61 (2001) 321-33.
[14] C. Schuecker, B.D. Davidson, Evaluation of the accuracy of the four-point bend end-notched flexure test for mode II delamination toughness determination, Composites Science and Technology, 60 (2000) 2137-46.
[15] H. Luo, Y. Yan, T. Zhang, Z. Liang, Progressive failure and experimental study of adhesively bonded composite single-lap joints subjected to axial tensile loads, Journal of Adhesion Science and Technology, 30 (2016) 894-914.
[16] A.U. Sane, P.M. Padole, C.M. Manjunatha, R.V. Uddanwadiker, P. Jhunjhunwala, Mixed mode cohesive zone modelling and analysis of adhesively bonded composite T-joint under pull-out load, Journal of the Brazilian Society of Mechanical Sciences and Engineering, 40 (2018) 167.
[17] R. Dimitri, M. Trullo, L. De Lorenzis, G. Zavarise, Coupled cohesive zone models for mixed-mode fracture: A comparative study, Engineering Fracture Mechanics, 148 (2015) 145-79.
[18] R.J.B. Rocha, R.D.S.G. Campilho, Evaluation of different modelling conditions in the cohesive zone analysis of single-lap bonded joints, The Journal of Adhesion, (2017) in press.
[19] A. Ameli, M. Papini, J.A. Schroeder, J.K. Spelt, Fracture R-curve characterization of toughened epoxy adhesives, Engineering Fracture Mechanics, 77 (2010) 521-34.
[20] M. Rhême, J. Botsis, J. Cugnoni, P. Navi, Influence of the moisture content on the fracture characteristics of welded wood joint. Part 2: Mode II fracture, Holzforschung, 67 (2013) 755-61.
[21] G. Ji, Z. Ouyang, G. Li, S. Ibekwe, S.-S. Pang, Effects of adhesive thickness on global and local Mode-I interfacial fracture of bonded joints, International Journal of Solids and Structures, 47 (2010) 2445-58.